Reaction Chemistry & Engineering

Linking fundamental chemistry and engineering to create scalable, efficient processes

Accepted Manuscript

This article can be cited before page numbers have been issued, to do this please use: A. Pankajakshan, S. G. Bawa, A. Gavriilidis and F. Galvanin, *React. Chem. Eng.*, 2023, DOI: 10.1039/D3RE00156C.

This is an Accepted Manuscript, which has been through the Royal Society of Chemistry peer review process and has been accepted for publication.

Accepted Manuscripts are published online shortly after acceptance, before technical editing, formatting and proof reading. Using this free service, authors can make their results available to the community, in citable form, before we publish the edited article. We will replace this Accepted Manuscript with the edited and formatted Advance Article as soon as it is available.

You can find more information about Accepted Manuscripts in the Information for Authors.

Please note that technical editing may introduce minor changes to the text and/or graphics, which may alter content. The journal's standard Terms & Conditions and the Ethical guidelines still apply. In no event shall the Royal Society of Chemistry be held responsible for any errors or omissions in this Accepted Manuscript or any consequences arising from the use of any information it contains.

View Article Online
DOI: 10.1039/D3RE00156C

Journal Name

ARTICLE TYPE

Cite this: DOI: 00.0000/xxxxxxxxxx

Autonomous kinetic model identification using optimal experimental design and retrospective data analysis: methane complete oxidation as a case study†

Arun Pankajakshan, Solomon Gajere Bawa, Asterios Gavriilidis,* and Federico Galvanin*

Received Date
Accepted Date

DOI: 00.0000/xxxxxxxxxx

Automation and feedback optimization are combined in a smart laboratory platform for the purpose of identifying appropriate kinetic models online. In the platform, model-based design of experiments methods are employed in the feedback optimization loop to design optimal experiments that generate data needed for rapid validation of kinetic models. The online sequential decision-making in the platform, involving selection of the most appropriate kinetic model structure followed by the precise estimation of its parameters is done by autonomously switching the respective objective functions to discriminate between competing models and to minimise the parametric uncertainty of an appropriate model. The platform is also equipped with data analysis methods to study the behaviour of models within their uncertainty limits. This means that the platform not only facilitates rapid validation of kinetic models, but also returns uncertainty-aware predictive models that are valuable tools for model-based decision systems. The platform is tested on a case study of kinetic model identification of complete oxidation of methane on Pd/Al_2O_3 catalyst, employing a micro packed bed reactor. A suitable kinetic model with precise estimation of its parameters was determined by performing a total of 20 automated experiments, completed in two days.

1 Introduction

The fast-proceeding digitalisation in process industries has led to the automation of decision-making processes in plant operations. This involves optimizations with high-fidelity and data-driven models that are continuously validated using data generated through feedback optimization loops. In the context of automated decision-making in chemical processes, decision-making often involves optimizations with high-fidelity kinetic models. Combining flow chemistry[1], microreactor technology[2,3] and computational methods have provided automated platforms for rapid development and identification of kinetic models. The methods employed in automated platforms for the development of kinetic models of chemical reactions fall into two categories: i) automated mechanism generation and model building and ii) automated model validation and refinement.

Some of the notable contributions in the first category include the Reaction Modelling Suite (RMS)[4], Reaction Mechanism Generator (RMG)[5,6] and Genesys[7,8]. All these works propose tools to automatically translate a set of chemistry rules into model equations and to validate the resultant models. A similar approach used for discovery of new synthetic routes is Computer Aided Synthesis Planning (CASP) which is a machine learning-assisted optimized search methodology to find feasible routes towards a target molecule, given the target molecule as the input[9–11]. In general, the automatic generation of chemical reaction mechanism and kinetic model structures using brute-force computing algorithms subjected to feasibility constraints will eventually reduce the redundant task of chemists or modellers in scripting down the model equations. It will also improve the level of knowledge abstraction between similar systems.

The second category of methods are focused on the automated validation of mechanistic or data-driven process models in smart laboratory platforms integrated with intelligent design with (closed loop) or without (open loop) feedback optimization. Significant contribution in this research field includes self-optimizing reaction systems[12–16] that mainly use Design of Experiments (DoE) methods[17–19] and regression models to optimize the process conditions in automated flow reactor systems. Another approach includes application of online Model-based De-

Department of Chemical Engineering, University College London, London, United Kingdom. Fax: XX XXXX XXXX; Tel: XX XXXX XXXX; E-mail: a.gavriilidis@ucl.ac.uk, f.galvanin@ucl.ac.uk

† Electronic Supplementary Information (ESI) available: [details of any supplementary information available should be included here]. See DOI: 00.0000/00000000.

‡ Additional footnotes to the title and authors can be included *e.g.* 'Present address:' or 'These authors contributed equally to this work' as above using the symbols: ‡, §, and ¶. Please place the appropriate symbol next to the author's name and include a `\footnotetext` entry in the the correct place in the list.

View Article Online
DOI: 10.1039/D3RE00156C

sign of Experiments (MBDoE) methods[20,21] in automated reactor platforms to optimally explore the design space to generate information-rich data needed for rapid validation of mechanistic kinetic models[22–30].

In this work, we report the development of an algorithmic and computational framework to achieve autonomous kinetic model identification in a smart microreactor platform for a heterogeneously catalysed gas/solid reaction. Here, the keyword *smart* means the microreactor system is fully automated and digitalised for our purpose and the keyword *autonomous* is used to indicate the platform is self-sufficient to identify and study appropriate kinetic models without any human intervention. Although similar platforms have been previously reported and successfully applied to solve real world problems of chemical kinetics[24,28], in this work we propose a framework in which the autonomous features necessary for kinetic model identification are powered by optimal experimental design and retrospective analysis of models. Another intention of the paper is to report a new Python Optimization Modeling Objects (Pyomo)[31–33] based parameter estimation module and a probability criterion for online model selection, both part of the proposed framework. The paper is organised as follows: i) In Section 2, the main modules of the smart laboratory platform with the theoretical details are discussed, ii) Section 3 introduces the case study of complete oxidation of methane along with the details of candidate kinetic models and the model reparameterisations used, iii) Section 4 discusses the results obtained and the major implications and iv) Section 5 provides a conclusion and future scope of the work.

2 Methods

The flowchart of the algorithmic and computational framework of the smart laboratory platform used for autonomous identification of kinetic models is shown in Figure 1. As shown in the figure, the platform is driven by a computational framework consisting of five modules: 1) Preliminary design module, 2) Resource module, 3) Model calibration module, 4) Autonomous decision module, and 5) Model-based design of experiments module. These five modules are operated in a loop until the goal of identifying a predictive kinetic model is achieved. An add-on to the platform is the retrospective data analysis module, which has been set up to review the results obtained by the platform, to reassess the decisions taken by the platform and to provide further insights or actions if needed.

2.1 Preliminary design module

The preliminary design module consists of pure statistical (model-free) DoE methods whose objective is to efficiently sample the experimental design space (the domain of possible values of the experimental conditions) for qualitative and quantitative purposes. The first qualitative purpose of DoE methods is to provide randomisation of experiments, meaning the experimental conditions must be independent of each other and should represent the entire design space. This is necessary to protect the principal assumption in estimation methods that the output data is a *random sample* of some infinite population that describes the whole characteristics of the system. Further qualitative benefits from DoE methods are: *i*) Greater efficiency, meaning the experimental sampling should provide more information about the system with less number of experiments and *ii*) Greater comprehensiveness, which means that the DoE sampling should result in experiments that help to understand the whole of the cause-effect relationships of the system[17]. The quantitative purpose of DoE sampling is to generate output data to be used for *i*) estimating the random error in observations, possibly from few repetitions of some experiments and *ii*) the primary validation of the proposed process models, i.e., to obtain an estimate of the model parameters and their statistical uncertainty. The latter is important in the robustness of the step of designing model-based optimal experiments, which is explained in the Design module of the platform. As shown in Figure 1, in this work, Factorial[17] DoE is used in the Preliminary design module. The Factorial arrangement of experiments in which the causing factors or inputs are varied over different discrete levels and the experiments consist of all possible combinations of these levels across all the factors, offers all the significant advantages stated above. However, one disadvantage of using a factorial design is the explosive growth of experiments with increasing number of factors and levels. As a solution, in higher dimensional experimental design space, two-level fractional factorial designs remain the preferred choice[34]. A generalised version of the traditional fractional factorial designs is the Generalized Subset Design (GSD)[34], which is appropriate for problems where factors have more than two levels.

2.2 Resource module

The execution of actual experiments in the smart laboratory platform will generate output data that are used to validate the set of proposed process models (the set of models corresponding to different hypothesised reaction mechanism). The set of proposed reaction process models are called identification models. The data together with the set of identification models comprise the Resource module of the smart laboratory platform (see Figure 1). The identification models of chemical reaction systems are commonly Differential and Algebraic Equations (DAEs), which can be represented in the following state-space form

$$\begin{aligned} &\mathbf{f}(\dot{\mathbf{x}}(t),\mathbf{x}(t),\mathbf{u}(t),\boldsymbol{\theta}) = \mathbf{0} \\ &\hat{\mathbf{y}}(t) = \mathbf{h}(\mathbf{x}(t),\mathbf{u}(t),\boldsymbol{\theta}) \\ &\mathbf{y}(t) = \mathbf{h}(\mathbf{x}(t),\mathbf{u}(t),\boldsymbol{\theta}) + \boldsymbol{\varepsilon} \qquad \boldsymbol{\varepsilon} \sim \mathcal{N}(\mathbf{0},\Sigma_{\mathbf{Y}}) \end{aligned} \tag{1}$$

In Equation 1, $\mathbf{x} \in \mathbb{R}^{N_x}$ is the vector of state variables, $\dot{\mathbf{x}}$ is the vector of first derivatives of the state variables, $\mathbf{u} \in \mathbb{R}^{N_u}$ is the vector of inputs or control variables that define the condition of an experiment, $\boldsymbol{\theta} \in \mathbb{R}^{N_\theta}$ is the vector of model parameters, $\hat{\mathbf{y}} \in \mathbb{R}^{N_{\hat{y}}}$ is the vector of model predictions of the outputs or response variables $\mathbf{y}$ (those state variables which are measured), $\mathbf{f}$ denotes the vector of functions representing the state equation and $\mathbf{h}$ denotes that of representing the output equation. In case of chemical reaction systems, both $\mathbf{f}$ and $\mathbf{h}$ are usually nonlinear functions of $\boldsymbol{\theta}$ and $\mathbf{u}$. The outputs $\mathbf{y}$ from different experiments result in a population

View Article Online
DOI: 10.1039/D3RE00156C

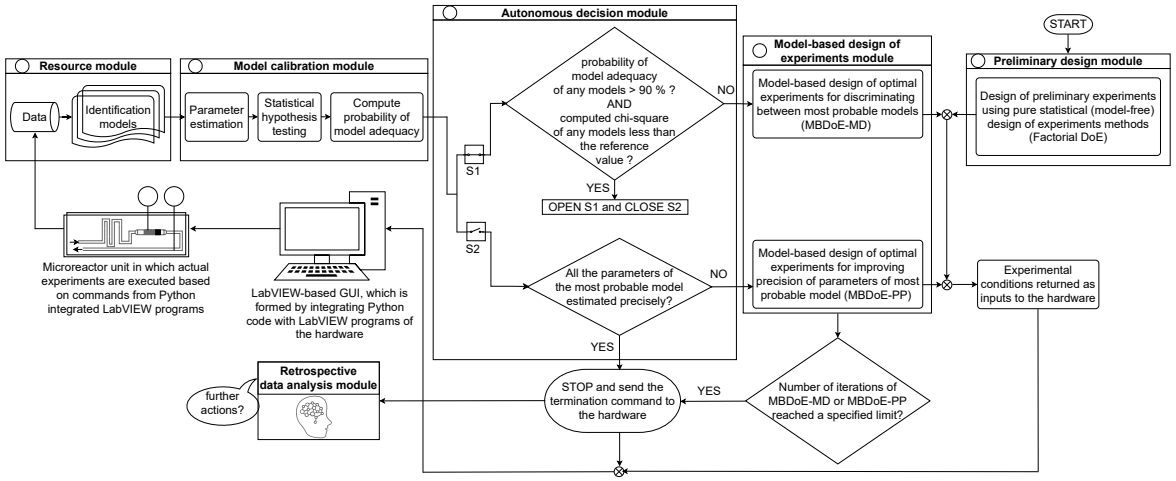

Fig. 1 Flowchart of the computational framework employed in the smart laboratory platform for online kinetic studies.

of data which can be learnt by repeating some experiments and calculating means and standard errors. The common practice is to assume that the measurement error ε follows an independent and identically distributed (i.i.d) Gaussian distribution with mean vector $\mathbf{0}$ and covariance matrix $\Sigma_{\mathbf{y}}$, which are then calculated from repeated experiments. We have also followed this approach here and more details about this can be found in our previous work[35].

2.3 Model calibration module

The objective of Model calibration module is to test if the identification models can represent the population of output data, i.e., to check if the models are able to describe the output data and its distribution. As seen in Figure 1, this module involves three class of methods: *i*) parameter estimation, *ii*) statistical hypothesis testing and *iii*) model selection by means of probability of model adequacy

2.3.1 Parameter estimation.

In the parameter estimation step, the identification models are used to fit the output data with the objective to estimate the unknown parameters of these models for which the models are able to describe the data within the limits of its learnt population. In this work, we have used the method of maximum likelihood[36,37] for parameter estimation. The method suggests that most probable values of the model parameters are those that maximises the likelihood function $\mathscr{L}(\theta|\mathbf{Y})$ given below

$$\mathscr{L}(\theta|\mathbf{Y}) = \prod_{i=1}^{n} p(\mathbf{y}_i|\theta) = \prod_{i=1}^{n} p(\mathbf{y}_i - \hat{\mathbf{y}}_i(\theta))$$

$$= \prod_{i=1}^{n} (2\pi)^{-N_y/2} \det{}^{-1/2}\Sigma_{\mathbf{Y}} \exp(-1/2[\mathbf{y}_i - \hat{\mathbf{y}}_i(\theta)]^{\top}\Sigma_{\mathbf{Y}}^{-1}[\mathbf{y}_i - \hat{\mathbf{y}}_i(\theta)]) \quad (2)$$

Note that the form of likelihood function provided in Equation 2 is based on the earlier assumptions $\varepsilon \sim \mathscr{N}(\mathbf{0}, \Sigma_{\mathbf{Y}})$ made about the measurement error distribution. In Equation 2, $\mathbf{Y}$ denotes the entire set of output data, $p(\cdot)$ denotes the probability density function and n denotes the total number of samples. As mentioned in Section 2.2, since $\mathbf{f}$ is usually nonlinear in θ, often the parameter estimation problems are nonlinear and nonconvex optimization problems with multiple local optima, sometimes including flat regions in the objective function because of poor parameter identifiability[38–40]. The effective solution of parameter estimation problem with a fast and good convergence is critical in online estimation methods. To tackle this, in this work, we have solved the parameter estimation problems using a code developed in Pyomo[31–33]. This implementation is particularly suited for solving parameter estimation with models represented by DAEs. The algorithm of this implementation is provided in Algorithm 1.

Parameter estimation using DAEs in Pyomo involves discretisation transformation of the DAEs into algebraic equations and then solving parameter estimation using the discretised models. The transformation of DAEs to algebraic equations is done by discretisation of the continuous domain of the DAEs and defining equality constraints to approximate derivatives at the discretisation points. In this work, orthogonal collocation[41] is used to discretise the continuous domain in the DAEs.

$$\mathbf{U} = \left[\begin{pmatrix} u_1(t_{i1}) & u_1(t_{i2}) & \dots & u_1(t_{if}) \\ u_2(t_{i1}) & u_2(t_{i2}) & \dots & u_2(t_{if}) \\ \vdots & \vdots & \ddots & \vdots \\ u_{N_u}(t_{i1}) & u_{N_u}(t_{i2}) & \dots & u_{N_u}(t_{if}) \end{pmatrix}_{i=1,\dots,N_{\text{exp}}} \right]$$

$$\mathbf{Y} = \left[\begin{pmatrix} y_1(t_{\text{sp}_{i1}}) & y_1(t_{\text{sp}_{i2}}) & \dots & y_1(t_{\text{sp}_{iN_{\text{spi}}}}) \\ y_2(t_{\text{sp}_{i1}}) & y_2(t_{\text{sp}_{i2}}) & \dots & y_2(t_{\text{sp}_{iN_{\text{spi}}}}) \\ \vdots & \vdots & \ddots & \vdots \\ y_{N_y}(t_{\text{sp}_{i1}}) & y_{N_y}(t_{\text{sp}_{i2}}) & \dots & y_{N_y}(t_{\text{sp}_{iN_{\text{spi}}}}) \end{pmatrix}_{i=1,\dots,N_{\text{exp}}} \right]$$

$$\mathbf{T}_{\text{sp}} = \left[\begin{pmatrix} t_{\text{sp}_{i1}} \\ t_{\text{sp}_{i2}} \\ \vdots \\ t_{\text{sp}_{iN_{\text{spi}}}} \end{pmatrix}_{i=1,\dots,N_{\text{exp}}} \right] \quad (3)$$

As shown in Algorithm 1, step 1 and 2 of the algorithm in-

View Article Online
DOI: 10.1039/D3RE00156C

volves developing helper functions to create Python dictionaries for defining inputs and outputs in the Pyomo model. Step 3 involves creating a sorted Python list of all sampling times, which is needed to define the discretisation points in the Pyomo model. The full set of inputs $\mathbf{U}$, outputs $\mathbf{Y}$ and sampling times $\mathbf{T}_{\text{sp}}$ from all the performed experiments, which are needed in steps 1-3 of the algorithm shall be provided as Python lists as given below. Step 4 of the algorithm involves developing the Pyomo model using the inputs, outputs and sampling times created in steps 1-3. The final step 5 involves the discretisation of the Pyomo model and the solution of the resulting Nonlinear Programming (NLP) problem to obtain the maximum likelihood estimates $\hat{\theta}_{\text{MLE}}$ of model parameters.

Algorithm 1: Parameter estimation with DAE models in Pyomo

Input: $\mathbf{U}$, $\mathbf{Y}$, $\mathbf{T}_{\text{sp}}$, Initial guess θ_0 and bounds Θ of model parameters
Output: Maximum likelihood estimate $\hat{\theta}_{\text{MLE}}$ of model parameters

1 **Step 1**: Create Python dictionaries for inputs. This is shown in lines 2 to 4. For time-independent inputs, index t can be omitted.
2 $u1dic = \{(i,t) : u_1(i,t) \quad \forall i \in [0,\ldots,N_{\text{exp}}-1] \ \forall t \in [0,t_{\text{if}}]\}$
3 $\vdots$
4 $uN_udic = \{(i,t) : u_{N_u}(i,t) \quad \forall i \in [0,\ldots,N_{\text{exp}}-1] \ \forall t \in [0,t_{\text{if}}]\}$
5 **Step 2**: Create Python dictionaries for response variables. This is shown in lines 6 to 8.
6 $y1dic = \{(i,t) : y_1(i,t) \quad \forall i \in [0,\ldots,N_{\text{exp}}-1] \ \forall t \in \mathbf{T}_{\text{sp}}[i]\}$
7 $\vdots$
8 $yN_ydic = \{(i,t) : y_{N_y}(i,t) \quad \forall i \in [0,\ldots,N_{\text{exp}}-1] \ \forall t \in \mathbf{T}_{\text{sp}}[i]\}$
9 **Step 3**: Create a unique sorted Python list of all sampling times. This is shown in lines 10 to 14.
10 $sampling = \text{list}()$
11 **for** $i = 0$ **to** $N_{exp}-1$ **do**
12 $\quad sampling$.extend $(\text{list}(\mathbf{T}_{\text{sp}}[i]))$
13 **end**
14 Define st such that $st =$ unique sorted list of $sampling$
15 **Step 4**: Create Pyomo model by declaring
16 Pyomo ContinuousSet to define the continuous time domain, which is initialsed using st created in **Step 3**
17 inputs $\mathbf{U}$ as indexed Pyomo parameters, initialsed using Python dictionaries created in **Step 1**
18 measurements $\mathbf{Y}$ as indexed Pyomo parameters, initialised using Python dictionaries created in **Step 2**
19 model parameters θ as indexed Pyomo variables, initialised using initial guess θ_0 and bounds Θ
20 differential state variables $\mathbf{x}(t)$ and their first derivatives $\dot{\mathbf{x}}(t)$ defined over all experiments
21 differential equations $\mathbf{f}(\dot{\mathbf{x}}(t),\mathbf{x}(t),\mathbf{u}(t),\theta) = \mathbf{0}$ as constraints, defined over all experiments
22 objective function given in Equation 2
23 **Step 5**: Transcription and solution
24 Apply orthogonal collocation method to discretise the continuous domain and the differential equations of the Pyomo model
25 Solve the resultant NLP generated by the discretised Pyomo model to obtain the estimate $\hat{\theta}_{\text{MLE}}$

2.3.2 Statistical hypothesis testing.

In this sub-module, methods of statistical hypothesis testing[17,42,43] are used to test the validity of the results of parameter estimation. Two statistical hypothesis tests are used to validate the results of parameter estimation. First test is the chi-square goodness of fit test[44] which is used to test whether the errors of fitting confirm or contradict the hypothesis of randomly distributed measurement errors ε. For this purpose, the test evaluates whether the distribution of residuals $(\mathbf{y}-\hat{\mathbf{y}})$ can be considered as a random sample of the specified error distribution $\varepsilon \sim \mathcal{N}(\mathbf{0},\Sigma_{\mathbf{Y}})$. The test is performed by computing the chi-square χ^2 statistic according to the equation

$$\chi^2 = \sum_{i=1}^{n} [\mathbf{y}_i - \hat{\mathbf{y}}_i(\theta)]^\top \Sigma_{\mathbf{Y}}^{-1} [\mathbf{y}_i - \hat{\mathbf{y}}_i(\theta)] \tag{4}$$

and comparing the computed value to the reference chi-square value $\chi^2_{\text{ref}} = \chi^2_{N-N_\theta}(1-\alpha)$, which is the value from a chi-square distribution with $(N-N_\theta)$ degrees of freedom and α significance level. Here, N represents the total number of observations, i.e. $N = n \cdot N_y$. If the computed chi-square value is greater than the reference value, the deviations $(\mathbf{y}-\hat{\mathbf{y}})$ are greater than twice the standard deviation of the error distribution and hence the model fails to describe the data. Otherwise, the model is regarded as adequate representation of the data. The second test is the Student's t-test[45], which is used to evaluate the statistical quality of parameter estimates. The aim of the test is to confirm from data, whether the variation in the parameter estimates are contradicted or explained by the variation within the data. The variation in the parameter estimates can be explained using the parameter covariance matrix $\mathbf{V}_\theta$ which is approximated as the inverse of observed Fisher Information Matrix (FIM) $\mathbf{H}_\theta$, which in turn is approximated as

$$\begin{aligned} \mathbf{H}_\theta &= \left[\mathbf{V}_\theta^0\right]^{-1} + \sum_{i=1}^{n} \left(\frac{d\hat{\mathbf{y}}_i}{d\theta}\right)^\top \Sigma_{\mathbf{Y}}^{-1} \left(\frac{d\hat{\mathbf{y}}_i}{d\theta}\right) \\ \mathbf{V}_\theta &= \mathbf{H}_\theta^{-1} \end{aligned} \tag{5}$$

In Equation 5, $\mathbf{V}_\theta^0$ is the prior covariance matrix and $\frac{d\hat{\mathbf{y}}_i}{d\theta}$ is the $N_y \times N_\theta$ parameter sensitivity matrix whose elements are the sensitivity coefficients that are first derivatives of dependent variables w.r.t model parameters. From the parameter covariance matrix, the test statistic t-value for the Student's t-test can be computed for each parameter estimate as

$$t_i = \frac{\hat{\theta}_i}{t_{N-N_\theta}(1-\alpha/2)\sqrt{\mathbf{V}_{\theta_{ii}}}} \qquad \forall i = 1,\ldots,N_\theta \tag{6}$$

In Equation 6, $\hat{\theta}_i$ is the estimate of the i-th model parameter, the denominator of the equation represents $(1-\alpha)100\%$ confidence interval around the parameter estimates and $\mathbf{V}_{\theta_{ii}}$ denotes the i-th diagonal element of the parameter covariance matrix. In the Student's t-test, the computed t-value of individual model parameter is compared to a reference value $t_{\text{ref}} = t_{N-N_\theta}(1-\alpha/2)$, which is the t-value from a two-tailed t-distribution with $(N-N_\theta)$ degrees of freedom and α significance level. For a parameter esti-

View Article Online
DOI: 10.1039/D3RE00156C

mate having large confidence interval compared to the estimated value, the computed t-statistic tends to be smaller than the reference value and the estimation of that parameter is not considered statistically precise. Parameters having t-values larger than the reference values are considered well estimated. Another important factor to consider while investigating the quality of parameter estimates is the parameter correlation matrix $\mathbf{C}_{\boldsymbol{\theta}}$ whose elements are defined by

$$C_{ij} = \frac{V_{\theta_{ij}}}{\sqrt{V_{\theta_{ii}}}\sqrt{V_{\theta_{jj}}}} \qquad \forall i, \forall j = 1, \ldots, N_\theta \tag{7}$$

If C_{ij} approaches 1, parameters are highly correlated (or -1 for anti-correlated), which makes their unique estimation difficult. In the case of perfect correlation $C_{ij} = 1$ or anti-correlation $C_{ij} = -1$, one parameter can be expressed as function of other. This will alter the degrees of freedom and cause the t-test to be invalid.

2.3.3 Probability of model adequacy.

In this sub-module, a probability criterion is proposed to assign probabilities to models based on their relative fitting quality. The need for defining such a probability criterion is to select the best model in situations where more than one model appears to be compatible with the same set of observations; a situation referred to as equifinality[46] or model indeterminacy by modellers[47]. A possible example of model indeterminacy in chemical systems can happen in kinetic models of heterogenous chemical reactions involving adsorption of a gas on a metal oxide catalyst surface[48]. In such systems, the adsorption is affected by the source of the gas and the catalytic properties of the exposed surface and in many cases a distinction between type of adsorption (dissociative or molecular) is less clear from observed concentration data. Even when the distinction is clear in the atomic scale or surface level, the observed similar behaviour in the bulk phase (use of error prone concentration measurements from the bulk phase) can render any validation or discrimination attempt between different models based on type of adsorption impossible[48]. Under such circumstances, using statistics for online model selection or discrimination appear a vague index, but the equivalent probability represents a clear and user-friendly index[49]. The probability of model adequacy proposed in this work is defined as

$$\mathrm{Pr}_j = \frac{\mathrm{Pr}\left(\chi_j^2 \leq \chi^2_{N-N_\theta}\right)}{\sum_{j=1}^{N_m} \mathrm{Pr}\left(\chi_j^2 \leq \chi^2_{N-N_\theta}\right)} \qquad \forall j = 1, \ldots, N_m \tag{8}$$

In Equation 8, Pr_j is the probability not to reject model j, assuming the null hypothesis that the distribution of residuals of model j is a random sample of the error distribution is true. The probabilities $\mathrm{Pr}(\cdot)$ in the numerator and denominator of the equation are the p-value of the chi-square goodness of fit test. The greater these probability values, the more points in the residual distribution are not contradicted by the distribution of the measurement error. In this work, a target probability of 90 % is set as the threshold probability to select the most appropriate kinetic model.

2.4 Autonomous decision module

In this module, the results of parameter estimation, statistical hypothesis testing and probability criterion are combined to make inferences regarding different identification models. The module contains two case (if-else) statements that are used to make decisions in the identification procedure. As shown in Figure 1, the two case statements are connected in parallel using switches S1 and S2. By default, S1 is closed and S2 is open. Hence, the first decision is being made regarding the adequacy of identification models based on the results of chi-square goodness of fit test and values of probability of model adequacy. When this condition is met, satisfying the threshold values of both chi-square goodness of fit test and values of probability of model adequacy, an appropriate model that is able to represent the data is been selected from the set of identification models. This will automatically make the switch S1 open and S2 closed. Therefore, the second case statement to analyse the statistical precision of parameter estimates get activated. In the second case statement, the t-values of model parameters are used to assess if the parameters of the selected model (the model with the highest probability value) are precisely estimated. The case statement asks for more evidence or data when the condition is not met or send termination command if the condition is met.

2.5 Model-based design of experiments module

In the event of limitation of evidence to make inferences from the autonomous decision module i.e., when the conditions in the autonomous decision module are not met, future experiments are optimally designed using MBDoE methods. This is the job of the model-based design of experiments module of the platform. The design of optimal experiments using MBDoE methods can be formulated as an optimization problem in which relevant model-based objective functions are optimized by acting on the experimental design vector $\boldsymbol{\varphi}$. The design vector $\boldsymbol{\varphi}$ contains the conditions of an experiment usually defined by the set of initial conditions $\mathbf{y}_0$ of the state variables, set of inputs $\mathbf{u}$, sensor locations or sampling times $\mathbf{t}_{\mathrm{sp}}$ and possibly duration of the experiment t_{f}, i.e.,

$$\boldsymbol{\varphi} = \left[\mathbf{y}_0, \mathbf{u}, \mathbf{t}_{\mathrm{sp}}, t_{\mathrm{f}}\right]^\top \tag{9}$$

As shown in Figure 1, in the event of not meeting the conditions of the first case statement, i.e., when the conditions $\chi^2 \leq \chi^2_{\mathrm{ref}}$ and the threshold probability of 90 % is not achieved for any of the identification models, optimal experiments for discrimination among the most probable models are designed using MBDoE for model discrimination (MBDoE-MD) methods. In this work, the objective function used in the MBDoE-MD method is the one proposed by Buzzi Ferraris et al.[50], which is maximised to obtain the optimal experimental condition for discriminating the most probable models. The MBDoE-MD problem is formulated as the optimization problem

$$\begin{aligned} &\max_{\varphi} \quad T_{ij}(\varphi) \\ &T_{ij}(\varphi) = [\hat{\mathbf{y}}(\boldsymbol{\varphi}, \hat{\boldsymbol{\theta}}_i) - \hat{\mathbf{y}}(\boldsymbol{\varphi}, \hat{\boldsymbol{\theta}}_j)]^\top \mathbf{V}_{ij}^{-1}(\boldsymbol{\varphi})[\hat{\mathbf{y}}(\boldsymbol{\varphi}, \hat{\boldsymbol{\theta}}_i) - \hat{\mathbf{y}}(\boldsymbol{\varphi}, \hat{\boldsymbol{\theta}}_j)] \end{aligned} \tag{10}$$

View Article Online
DOI: 10.1039/D3RE00156C

In Equation 10, T_{ij} is the objective function that is maximised to discriminate between models i and j; T_{ij} represents the deviation between predictions $\hat{\mathbf{y}}(\boldsymbol{\varphi},\hat{\boldsymbol{\theta}}_i)$ and $\hat{\mathbf{y}}(\boldsymbol{\varphi},\hat{\boldsymbol{\theta}}_j)$ of the two models i and j relative to the limits of error in the predictions, denoted by $\mathbf{V}_{ij}^{-1}(\boldsymbol{\varphi})$, which is the covariance matrix of the random variable $\delta_i(\boldsymbol{\varphi})-\delta_j(\boldsymbol{\varphi})$, where $\delta_i(\boldsymbol{\varphi})=\hat{\mathbf{y}}(\boldsymbol{\varphi},\hat{\boldsymbol{\theta}}_i)-\mathbf{y}$ and $\delta_j(\boldsymbol{\varphi})=\hat{\mathbf{y}}(\boldsymbol{\varphi},\hat{\boldsymbol{\theta}}_j)-\mathbf{y}$. The covariance matrix $\mathbf{V}_{ij}(\boldsymbol{\varphi})$ is computed as

$$\begin{aligned}&\mathbf{V}_{ij}(\boldsymbol{\varphi})=\mathbf{V}_{\hat{\mathbf{y}}}(\boldsymbol{\varphi},\hat{\boldsymbol{\theta}}_i)+\mathbf{V}_{\hat{\mathbf{y}}}(\boldsymbol{\varphi},\hat{\boldsymbol{\theta}}_j)+2\Sigma_{\mathbf{y}}\\&\text{where},\mathbf{V}_{\hat{\mathbf{y}}}(\boldsymbol{\varphi},\hat{\boldsymbol{\theta}})=\left(\frac{d\hat{\mathbf{y}}(\boldsymbol{\varphi})}{d\boldsymbol{\theta}}\right)\mathbf{V}_{\boldsymbol{\theta}}\left(\frac{d\hat{\mathbf{y}}(\boldsymbol{\varphi})}{d\boldsymbol{\theta}}\right)^{\top}\Bigg|_{\boldsymbol{\theta}=\hat{\boldsymbol{\theta}}}\end{aligned}\tag{11}$$

As shown in Figure 1, in the event of not meeting a statistically precise estimation of parameters of the most probable model (the model with probability of model adequacy > 90 %), optimal experiments for improving precision of model parameters are designed using MBDoE for improving parameter precision (MBDoE-PP)[21]. The MBDoE-PP problem is formulated as an optimization problem of the type

$$\min_{\boldsymbol{\varphi}}\quad \psi\left(\left[\mathbf{H}_{\boldsymbol{\theta}}+\hat{\mathbf{H}}_{\boldsymbol{\theta}}\left(\boldsymbol{\varphi},\hat{\boldsymbol{\theta}}\right)\right]^{-1}\right)\tag{12}$$

In Equation 12, $\mathbf{H}_{\boldsymbol{\theta}}$ is the observed FIM, $\hat{\mathbf{H}}_{\boldsymbol{\theta}}(\cdot)$ is the expected FIM and $\psi(\cdot)$ is the objective function, which is a metric of the parameter covariance matrix. Classical choice of ψ is the alphabetical (A-, E- and D-optimal) design criteria[51]. In this work, we have used the D-optimal design criterion as the objective function for MBDoE-PP, which corresponds to the minimisation of the determinant of the parameter covariance matrix.

2.6 Retrospective data analysis module

This module has been considered as an add-on in the autonomous platform to mimic a human brain in analysing the results obtained by the platform and to review the decisions made by the platform. In fact in all automated platforms, there is a chance that a false decision can be made whenever the real effects are obscured by various errors such as observational errors or errors in validation. This happens in general when the real effects are small relative to such errors. In the autonomous platform for kinetic model identification, even if the decisions taken (online parameter estimation and MBDoE) are continuously reviewed and updated in the light of fresh data, the decisions can be affected by two intrinsic limitations of the MBDoE methods. Firstly, these methods are based on large-sample theory; in particular, the validation step involving statistical hypothesis testing are truly valid at asymptotic conditions of data. Therefore, the decisions made at early stages are relatively error-prone. Secondly, the validation procedures are based on the current value of parameter estimates without looking at the uncertainty regions of parameter estimates. To tackle these limitations, and to enhance the cognitive limits of autonomous platforms to make right decisions, we propose a retrospective analysis of data as well as models within the limits of their uncertainty.

In the retrospective data analysis, we evaluate the model prediction density plots by approximating the probability distributions of model predictions. This can be done in two ways. In the first method, for each experimental condition, the sampling distributions of model predictions can be approximated as multivariate normal distribution with mean vector $\hat{\mathbf{y}}$ and covariance matrix $\mathbf{V}_{\hat{\mathbf{y}}}$, computed using Equation 11. In this method, the prediction density plots for each experimental condition represent a random sample drawn from the multivariate normal distribution $\mathcal{N}_{N_y}\left(\hat{\mathbf{y}}_i,\mathbf{V}_{\hat{\mathbf{y}}_i}\right)$, where i represents a sampling point. In the second method, random sample of parameter vectors are first generated by sampling from a multivariate normal distribution with mean vector $\hat{\boldsymbol{\theta}}$ and covariance matrix $\mathbf{V}_{\boldsymbol{\theta}}$, $\mathcal{N}_{N_\theta}(\hat{\boldsymbol{\theta}},\mathbf{V}_{\boldsymbol{\theta}})$. Then the model predictions are evaluated for each observation of this random sample, and the prediction density plot for each experimental condition and for each output variable is approximated from the histogram of the model predictions. In the first method we have to make an assumption about the probability distribution of the model predictions, while the latter method does not need such an assumption. In this work, we have chosen the latter method for generating prediction density plots.

3 Case Study - Complete Catalytic Oxidation of Methane

In this work, the smart laboratory platform was demonstrated for the automated identification of an appropriate kinetic model for the methane complete oxidation over 5 wt.% Pd/Al_2O_3 catalyst.

$$CH_4+2O_2\xrightarrow{Pd/Al_2O_3}CO_2+2H_2O$$

The kinetic study was conducted using 10 mg of 69 μm average size catalyst in a micropacked bed reactor operated at steady state and automatically controlled using LabVIEW[52–54].

3.1 Experimental set-up

The silicon-glass microreactor was fabricated using photolithography, deep reactive ion etching and anodic bonding. The reaction channel was 0.42 and 2 mm deep and wide respectively, and contained the catalyst for the reaction. The catalyst was held in place in the reaction zone by a retainer, present at the end of the reaction zone. The microreactor could be employed for reaction up to a maximum temperature of 400 °C. For temperature monitoring within the catalyst bed, the reactor had six deed-end slots for inserting K-type thermocouples. Further details are available in our previous work[35]. A schematic of the experimental set-up is shown in Figure 2. The composition of the inlet stream was made up of 5 % methane in helium, oxygen and nitrogen as internal standard. The pressure was monitored with pressure sensors (Honeywell, 40PC, 100 psig). To maintain a constant desired reactor outlet pressure, a pressure controller (Brooks, 5866) was placed after the microreactor. The mole fractions of methane, oxygen and carbon dioxide were measured with an online gas chromatograph (Agilent, 7890A), equipped with pneumatic sampling valve, sampling loop, GS-Carbon PLOT (Agilent), HP-PLOT molecular sieve (Agilent) and thermal conductivity detector. Hardware automation was achieved by integration

View Article Online
DOI: 10.1039/D3RE00156C

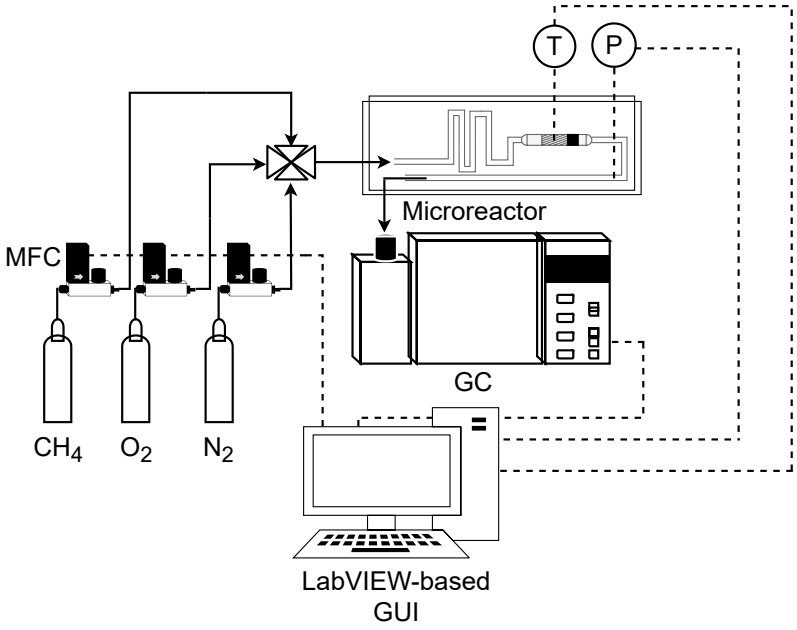

Fig. 2 Schematic of the methane complete catalytic oxidation system. MFC: mass flow controller, T: temperature controller, P: pressure controller and GC: gas chromaograph. The solid lines indicate gas flow paths, the dashed lines indicate control/measured signals.

of all the hardware components by means of Python-LabVIEW. In the automated procedure, the gas chromatograph automatically saved the measured data in an Excel file. A Python code was used to access this file and save the measured data in another Excel file called record file. The experimental conditions were also saved in the record file. The record file was updated after each experiment and the updated file was used as the data source for parameter estimation algorithm. Using the Timed loop in LabVIEW, the duration for each experiment, which comprised of the reaction time and the analysis time in the gas chromatograph was set at 20 minutes. The solid lines in Figure 2 show the gas flow paths. The dashed lines represent the communication of control/measured signals of the mass flow controllers, the temperature controller, the pressure controller and the gas chromatograph. The control signals are the signals sent from the LabVIEW-based Graphical User Interface (GUI) to the control devices. The measured signals are the signals read from different sensors, which are displayed on the GUI. Further details on the development of automated experimental platform are available in[35].

3.2 Mass and heat transfer resistances

The reaction system was assumed to be unaffected by mass transfer resistances, which was verified by computing the Mear's criterion and the Weisz-Prater number[55] for external and internal mass transfer resistances respectively. The most severe experimental conditions of high temperature and high reactant concentrations was used for the Mear's criterion calculation and a value of 0.026 (which is less than 0.15) was obtained, suggesting that external mass transfer limitation can be ignored. For the internal mass transfer resistance calculation, the Weisz-Prater criterion evaluation resulted to a value of 0.13, (which was less than 1), suggesting that the internal mass transfer resistance can

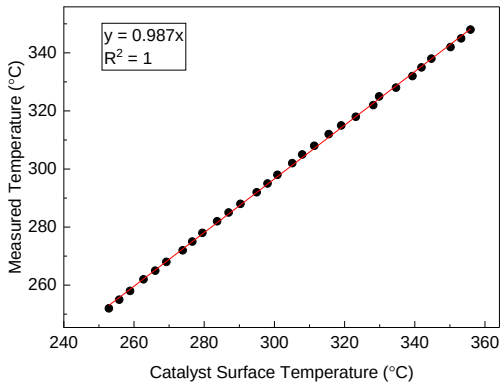

Fig. 3 Calculated catalyst particle surface temperature against measured temperature in the microreactor for catalytic methane combustion.

be neglected. More details about these calculations are provided in our previous work[35]. The criterion for isothermal condition within the catalyst particles was also satisfied, based on the condition that the observed rate of reaction must not differ more than 5 % from the actual reaction rate within the catalyst particle at constant temperature. According to the Mear's criterion for external heat transfer resistance, a value < 0.15 implies external heat transfer limitation could be neglected. The value obtained was 0.3, hence there was a need to estimate the catalyst surface temperature (T_s) from the measured temperature (T_m). A correlation shown in Figure 3 based on the preliminary data was used to develop a relationship between T_m and T_s, which was obtained as a linear relationship given in Figure 3. Detailed discussion on external heat transfer limitations and on the justification to use a linear relationship to correlate catalyst surface temperature and measured reactor temperature are provided in the supporting information of our previous work[35]. The linear relationship

View Article Online
DOI: 10.1039/D3RE00156C

Table 1 Range of control variables. Temperature is measured in the reactor, while all the other variables are at the reactor inlet.

Control variable	Temperature [°C]	Mass flow rate [Nml min^{-1}]	Oxygen to methane mole ratio [mol mol^{-1}]	Methane concentration [mol mol^{-1}]
Range	250-350	20-30	2-4	0.005-0.025

shown in Figure 3 was deployed within LabVIEW for regulating the temperature controller by reading the measured temperature rather than the catalyst surface temperature. However, the catalyst surface temperature was used for the kinetic studies. Axial dispersion was assumed to be negligible in the packed bed reactor based on the calculated aspect ratio. More information about the experimental set-up and reaction system can be found in our previous work[35].

3.3 Reactor model

With the assumptions stated above, the micro packed bed reactor was modelled as isothermal Plug Flow Reactor (PFR)[35] using the following set of Ordinary Differential Equations (ODEs)

$$\begin{aligned}
\frac{dx_1}{dw} &= \frac{R\cdot u_1}{u_2 P_{\text{avg}}}\cdot(-r) \quad x_1(0) = u_4 \\
\frac{dx_2}{dw} &= \frac{R\cdot u_1}{u_2 P_{\text{avg}}}\cdot(-2r) \quad x_2(0) = u_3\cdot u_4 \\
\frac{dx_3}{dw} &= \frac{R\cdot u_1}{u_2 P_{\text{avg}}}\cdot(r) \\
\frac{dx_4}{dw} &= \frac{R\cdot u_1}{u_2 P_{\text{avg}}}\cdot(2r) \\
y_i &= x_i \quad i = 1,2,3
\end{aligned} \tag{13}$$

In Equation 13, the state variables x_1, x_2, x_3 and x_4 represent the mole fraction [mol mol^{-1}] of methane, oxygen, carbon dioxide and water respectively. The control variables in the process include the reaction temperature [°C], flow rate of the feed [Nml min^{-1}], oxygen to methane mole ratio in the feed [mol mol^{-1}] and inlet methane mole fraction [mol mol^{-1}] which are respectively denoted as u_1, u_2, u_3 and u_4. These controls form the design vector $\boldsymbol{\varphi}$, which defines the conditions of an experiment. The design vector $\boldsymbol{\varphi}$ is bounded within the experimental design domain shown in Table 1. In Equation 13, R[J mol^{-1} K^{-1}] is the universal gas constant, r[mol g^{-1} min^{-1}] represents the reaction rate according to a postulated kinetic model, w[g] is the catalyst mass along the packed bed reactor (the domain of independent variable) and P_{avg}[bar] is the average pressure along the packed bed reactor, which was estimated using a pressure drop model[35].

The steady state mole fractions of methane, oxygen and carbon dioxide at the reactor outlet, measured across the performed experiments formed the output data set $\mathbf{Y}$. The random error in observations was computed from repeated measurements using the method of pooled standard deviation[35] and the covariance matrix of measurement error was estimated as

$$\Sigma_{\mathbf{y}} = \begin{bmatrix} 1.85\times10^{-7} & 0 & 0 \\ 0 & 4.08\times10^{-6} & 0 \\ 0 & 0 & 2.60\times10^{-7} \end{bmatrix} \tag{14}$$

The diagonal entries of the matrix $\Sigma_{\mathbf{y}}$ are the variances of random measurement error associated with measurement of methane, oxygen, and carbon dioxide mole fractions respectively.

3.4 Candidate kinetic models

Based on the results of a preliminary screening of kinetic models, which is discussed in[35], three candidate kinetic models were considered as the potential models to describe the methane complete oxidation reaction. The reaction mechanisms governing the models and the respective rate laws are provided in Table 2.

3.5 Reparametrisation of kinetic parameters

In order to minimise the correlation between kinetic parameters and to scale all the parameters to comparable magnitudes, the Arrhenius (Equation 15) and Van't Hoff (Equation 16) equations used in the kinetic models were reparametrised[58,59] as

$$k(T) = \exp\left(\log k(T_{\text{ref}}) - \frac{Ea}{R}\left(\frac{1}{T} - \frac{1}{T_{\text{ref}}}\right)\right) \tag{15}$$

$$K(T) = \exp\left(\log K(T_{\text{ref}}) - \frac{\Delta H}{R}\left(\frac{1}{T} - \frac{1}{T_{\text{ref}}}\right)\right) \tag{16}$$

In Equation 15, $k(T)$ is the reaction rate constant at temperature T, Ea is the activation energy and $T_{\text{ref}} = 320\ ^{\circ}C$ is the reference temperature. Similarly, in Equation 16, $K(T)$ is the equilibrium constant of adsorption at temperature T and ΔH is the enthalpy of adsorption. The actual parameters, units, and their reparametrised form for each of the candidate kinetic models are listed in Table 3. Instead of estimating the actual kinetic model parameters, the reparametrised parameters were estimated in the parameter estimation step.

3.6 Computational resources

All the computational procedures used in this work were performed on a 64-bit Windows machine with Intel®Core™i7-8550U CPU, 2.00GHz Processor and 8.00 GB RAM. The Python model identification framework was built in Python version 3.7.4. In the Python framework, pyDOE2 package[60] was used for the design of preliminary factorial experiments. The candidate kinetic models described by set of ODEs were written as Python functions. Solution of ODEs and simulation of the models including the computation of sensitivity functions were carried out using the odeint function within the Scipy[61] package (scipy.integrate.odeint) with lsoda[62] integrator. Parameter estimation was carried out in

View Article Online
DOI: 10.1039/D3RE00156C

Table 2 Candidate kinetic models considered in this work

Model	Description	Rate law
Model 1	Power law model	$r_{CH_4} = k_1 P_{CH_4}$
Model 2	Langmuir Hinshelwood (LH) mechanism (surface reaction between adsorbed methane and dissociatively chemisorbed oxygen[56,57])	$r_{CH_4} = \frac{k_r K_{CH_4} P_{CH_4} \sqrt{K_{O_2} P_{O_2}}}{\left(1+K_{CH_4} P_{CH_4}+\sqrt{K_{O_2} P_{O_2}}\right)^2}$
Model 3	Mars van Krevelen (MVK) mechanism (slow desorption of the reaction products[56,57])	$r_{CH_4} = \frac{k_1 k_2 P_{CH_4} P_{O_2}}{k_1 P_{O_2}+2k_2 P_{CH_4}+(k_1 k_2/k_3) P_{O_2} P_{CH_4}}$

Table 3 Actual parameters, units, and their reparametrised form in each of the kinetic models

Model	Actual parameter	Unit	Reparametrised form
Model 1	k_1	$mol\,bar^{-1}\,g^{-1}\,min^{-1}$	$\theta_1 = -\log k_1\,(T_{ref})$
	Ea_1	$J\,mol^{-1}$	$\theta_2 = \frac{Ea_1}{10^4}$
Model 2	k_r	$mol\,g^{-1}\,min^{-1}$	$\theta_1 = -\log k_r\,(T_{ref})$
	Ea_r	$J\,mol^{-1}$	$\theta_2 = \frac{Ea_r}{10^4}$
	K_{O_2}	bar^{-1}	$\theta_3 = \log K_{O_2}\,(T_{ref})$
	ΔH_{O_2}	$J\,mol^{-1}$	$\theta_4 = \frac{-\Delta H_{O_2}}{10^4}$
	K_{CH_4}	bar^{-1}	$\theta_5 = \log K_{CH_4}\,(T_{ref})$
	ΔH_{CH_4}	$J\,mol^{-1}$	$\theta_6 = \frac{-\Delta H_{CH_4}}{10^4}$
Model 3	k_1	$mol\,bar^{-1}\,g^{-1}\,min^{-1}$	$\theta_1 = -\log k_1\,(T_{ref})$
	Ea_1	$J\,mol^{-1}$	$\theta_2 = \frac{Ea_1}{10^4}$
	k_2	$mol\,bar^{-1}\,g^{-1}\,min^{-1}$	$\theta_3 = -\log k_2\,(T_{ref})$
	Ea_2	$J\,mol^{-1}$	$\theta_4 = \frac{Ea_2}{10^4}$
	k_3	$mol\,g^{-1}\,min^{-1}$	$\theta_5 = -\log k_3\,(T_{ref})$
	Ea_3	$J\,mol^{-1}$	$\theta_6 = \frac{Ea_3}{10^4}$

Pyomo using the Interior Point OPTimizer (IPOPT) solver[63]. The MBDoE problems were solved using the Sequential Least SQuares Programming (SLSQP)[64] solver in the minimize function in Scipy.optimize class.

4 Results and Discussion

Given the candidate kinetic models as input, the autonomous platform was able to perform unmanned experiments until the appropriate kinetic model of methane complete oxidation was identified. The experimental settings used by the platform in order to achieve this task comprised a campaign of Factorial experiments (Experiments 1-12) designed using two-level fractional factorial DoE method, MBDoE-MD experiments (Experiments 13 and 14) and MBDoE-PP experiments (Experiments 15-20). The experimental conditions of theses campaigns are shown in Figure 4. The full set of experimental data are provided in the electronic supplementary information.

4.1 Preliminary factorial experiments and first parameter estimation

As shown in Figure 4, the Factorial experiments consisted of two 2-level fractional factorial designs; one in which the ranges of input variables specified in Table 1 were used as levels and in the other where the same ranges were used as levels except for the inlet methane concentration for which a lower level of 0.015 was used. The experiments which were common in both the 2-level fractional factorial designs were performed only once. The autonomous operation of the platform did not start until the Factorial experiments were finished. The output data from the Factorial experiments was used for the first online parameter estimation. The results of first online parameter estimation are given in Table 4. It can be seen from the table that at the end of Factorial experiments, i.e., at the end of experiment 12, Model 1 (power law model) showed poor data compatibility and failed the chi-square goodness of fit test. Whereas, both Model 2 LH and Model 3 MVK passed the chi-square goodness of fit test, however with almost same chi-square values. This resulted in almost equal probabilities (≈ 50 %) for both the models. Immediately the Autonomous decision module and the Model-based design of experiments module of the platform were triggered to design new MBDoE experiments for discriminating between Model 2 and Model 3.

Table 4 Parameter estimation results showing chi-square and probability of model adequacy for candidate models at the end of Factorial campaign of experiments, i.e., at the end of experiment 12. The values in bold indicate a failure of the chi-square test, which happens when the computed value of chi-square becomes greater than the reference chi-square value.

Model	Adequacy χ^2/χ^2_{ref}	Probability of model adequacy (%)
Model 1	**63.34/48.60**	0.11
Model 2	23.63/43.77	51.64
Model 3	24.75/43.77	48.25

4.2 MBDoE assisted experiments and decisions made by the autonomous decision module

The parameter estimation results showing the chi-square values and the probability values for all the candidate models at the end of MBDoE-MD experiments are shown in Table 5. The same results can be read from the adequacy graph provided in Figure

View Article Online
DOI: 10.1039/D3RE00156C

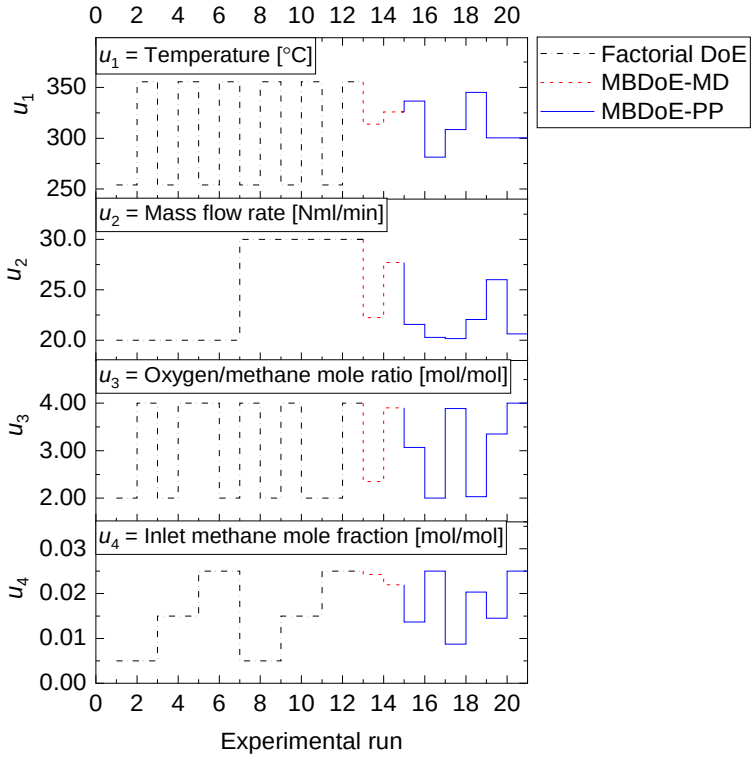

Fig. 4 Experimental conditions in Factorial, MBDoE-MD and MBDoE-PP campaign of experiments, used by the autonomous platform for identification of an appropriate kinetic model for methane oxidation.

Table 5 Parameter estimation results showing chi-square and probability of model adequacy for candidate models at the end of MBDoE-MD campaign of experiments, i.e., at the end of experiment 14. The values in bold indicate a failure of the chi-square test, which happens when the computed value of chi-square becomes greater than the reference chi-square value.

Model	Adequacy χ^2/χ^2_{ref}	Probability of model adequacy (%)
Model 1	**142.96/55.76**	0
Model 2	**54.80/50.99**	6.83
Model 3	39.52/50.997	93.17

Table 6 Parameter estimation results showing the estimated values, 95 % confidence interval (C.I) and t-values of parameters of Model 3 at the end of MBDoE-MD experimental campaign. Note that the value of t_{ref} is 1.68

Parameter	Estimate $\pm$95%C.I	t-value
θ_1	5.99 ± 0.39	15.14
θ_2	6.93 ± 3.59	1.93
θ_3	4.00 ± 2.54	1.57
θ_4	9.31 ± 20.05	0.46
θ_5	10.48 ± 0.20	51.26
θ_6	7.04 ± 1.79	3.94

5. The MBDoE-MD campaign of experiments started from experiment 13 and continued until the chi-square criterion $(\chi^2 < \chi^2_{ref})$ and the probability criterion $(\mathrm{Pr}_j > 90\,\%)$ confirmed a satisfactory discrimination between the models. This was achieved at the end of experiment 14, when Model 3 (MVK model) was found to be the most appropriate kinetic model, which agrees with the results of similar studies in literature[57]. It is interesting to see from Figure 4 that high temperature $(T > 300^\circ\mathrm{C})$, high oxygen to methane mole ratio $(\approx 4\,\mathrm{mol\,mol^{-1}})$ and high inlet methane mole fraction $(\approx 0.02\,\mathrm{mol\,mol^{-1}})$ resulted in discriminating between Model 2 and Model 3. This agrees with the literature suggesting that high methane concentration and high temperature promotes the rate of surface reduction and surface re-oxidation steps in the MVK mechanism, which is the striking difference between the LH and MVK mechanisms i.e., between Model 2 and Model 3[56,57]. It can be seen from both Table 5 and Figure 5 that at the end of experiment 14, only Model 3 passed the chi-square test with a probability value of 93 %. This automatically moved switch S1 to open position and S2 to closed position (see Figure 1), by selecting Model 3 as the appropriate model. At this stage, except parameter 3 and 4 (underlined in Table 6), all the parameters of Model 3 were estimated precisely according to the Student's t-test. The statistical precision of parameter estimates of Model 3 at the end of MBDoE-MD campaign of experiments can be also read from the graph of 95 % confidence intervals and t-values of parameter estimates, shown in Figure 6. The failure of t-test for parameter 3 and 4, triggered the MBDoE-PP methods to design new experiments for improving the precision of parameter estimates. The MBDoE-PP experiments started from experiment 15 and continued until all the parameters of Model 3 passed the t-test. This was achieved at the end of experiment 20. It can be seen from Table 7 and Figure 6 that at the end of experiment 20, all the parameters of Model 3 passed the t-test and the 95 % confidence interval for all parameter estimates have become narrow positive sets.

View Article Online
DOI: 10.1039/D3RE00156C

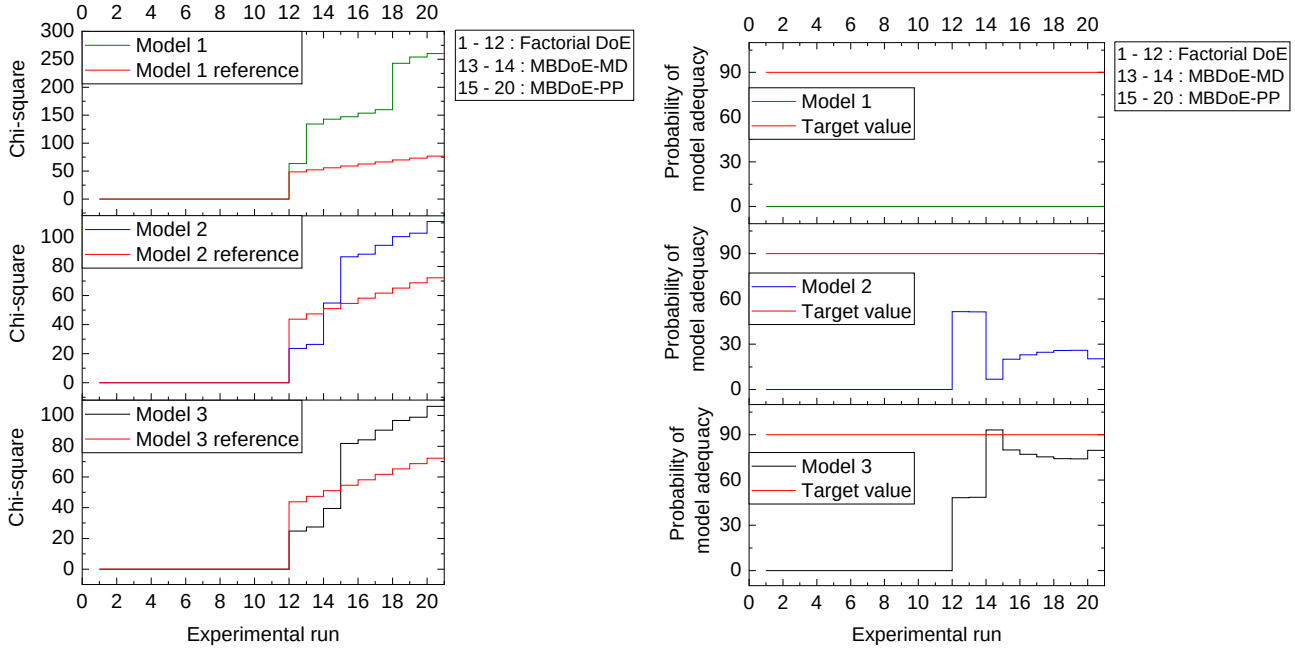

(a) Chi-square **(b)** Probability of model adequacy

Fig. 5 Chi-square value and probability of model adequacy computed for candidate models in the experimental runs in the campaigns indicated.

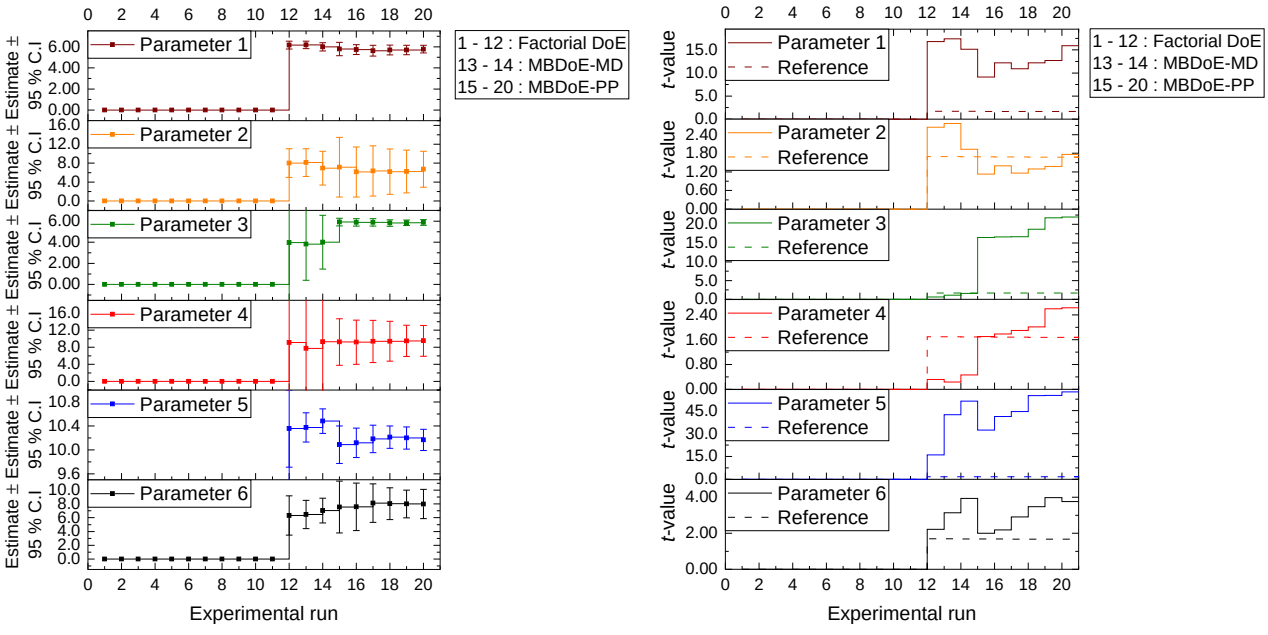

(a) 95 % confidence interval **(b)** *t*-value

Fig. 6 Confidence interval (95 %) and *t*-value for parameter estimates of Model 3, updated in the experimental runs in the campaigns indicated.

View Article Online
DOI: 10.1039/D3RE00156C

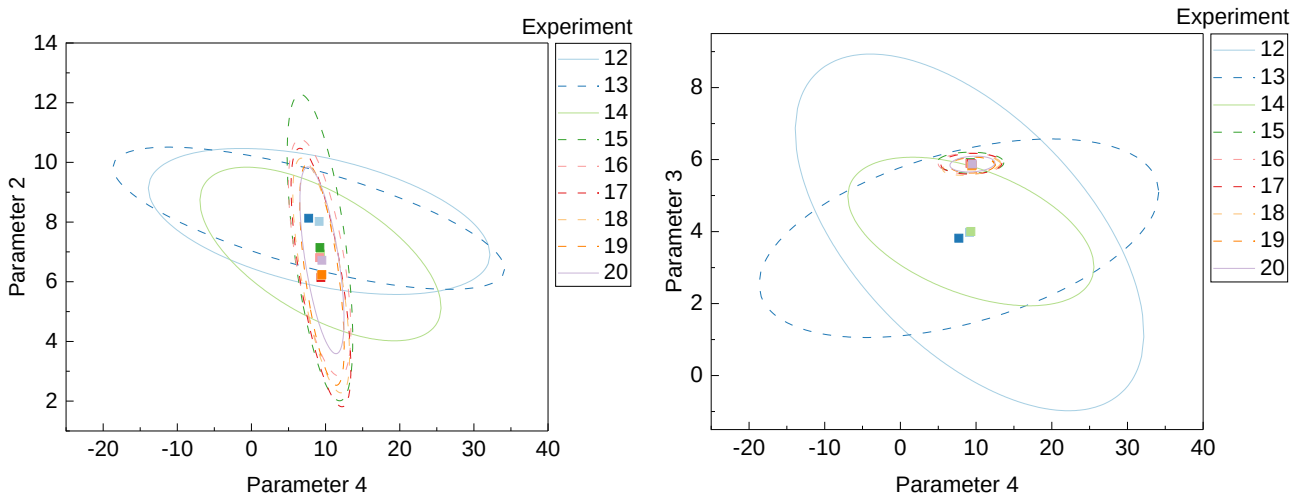

(a) Parameter 2 and 4 **(b)** Parameter 3 and 4

Fig. 7 Confidence ellipses for critical parameter pairs of Model 3, at the end of the experiment indicated.

Table 7 Parameter estimation results showing the estimated values, 95 % confidence interval (C.I) and *t*-values of parameters of Model 3 at the end of MBDoE-PP experimental campaign. Note that the value of t_{ref} is 1.67

Parameter	Estimate ± 95%C.I	*t*-value
θ_1	5.77 ± 0.36	15.91
θ_2	6.72 ± 3.81	1.76
θ_3	5.87 ± 0.27	21.94
θ_4	9.51 ± 3.62	2.62
θ_5	10.17 ± 0.18	57.38
θ_6	7.98 ± 2.12	3.76

Although parameters 3 and 4 initially appeared to be the critical parameters, which were not estimated precisely at the end of MBDoE-MD campaign, further experimentation proved that parameters 2 and 4 were the critical parameters. The 95 % confidence ellipse showing the uncertainty regions of parameter pairs (2 and 4) and (3 and 4) are shown in Figure 7. A careful evaluation of the confidence ellipses in Figure 7 suggests that the experiment 15 (high temperature 327 °C and high oxygen to methane mole ratio 4) significantly reduced the uncertainty region of parameter 4, which is the activation energy of the surface reduction step in Model 3. Whereas, experiment 20 resulted in reducing the size of uncertainty region of parameter 2, which is the activation energy of surface oxidation step of Model 3. Another interesting result regarding the correlation between parameters of Model 3 at the end of Factorial, MBDoE-MD and MBDoE-PP experimental campaign are shown in Figure 8. It can be observed from the figure that none of the parameters had perfect correlation or anti-correlation. Moreover, the correlation between the parameters was relatively reduced in the course of experimentation, suggesting good validity of *t*-test.

The values of reaction rate constant (at the reference temperature), pre-exponential factor and activation energy for different steps of Model 3 were obtained from the final parameter estimates of Model 3. These values are provided in Table 8. A comparison of the reaction rate constants at the reference temperature (320 °C) indicates that the slowest step in the mechanism is the desorption of products, which agrees with the assumptions of Model 3. In addition, the values of activation energies for surface oxidation and desorption of products, obtained in this study (67.2 ± 38.1, 79.8 ± 21.2) kJ mol^{-1} are comparable (considering the uncertainty limit) to those (51.5, 108.5) kJ mol^{-1} obtained for the oxidation of methane over commercial 0.5 % Pd on $\gamma - Al_2O_3$ [57]. However, the activation energy for the surface reduction step obtained in this work (95.1 ± 36.2 kJ mol^{-1}) is higher than that (16.8 kJ mol^{-1}) reported in the literature [57].

4.3 Retrospective analysis of models

It shall be noted that at the end of MBDoE-PP experimental campaign, both Model 2 and Model 3 failed the chi-square goodness of fit test. This is clearly shown in the adequacy graph of Figure 5. In addition, the computed chi-square values were very close for both the models, indicating their similar behaviour. This led to the retrospective analysis of the models using prediction density plots as well as residual plots. The prediction density plots for Model 2 and 3 were created based on the methods discussed in section 2.6. The joint prediction density plots of Model 2 and 3 using the final parameter estimates were created for each experimental condition and for each of the output variables. This analysis aimed to better study the degree of discrimination between the two models.

The joint prediction density plots of the models along with the experimental observation within its error bound suggested that it is very difficult to discriminate between Model 2 and 3 using the observables. In most of the cases, the degree of discrimination was found negligible compared to the magnitude of random error in observations. The full set of prediction density plots are provided in the electronic supplementary information. The case where the degree of discrimination between the models is at least as significant as the error in observation was obtained

View Article Online
DOI: 10.1039/D3RE00156C

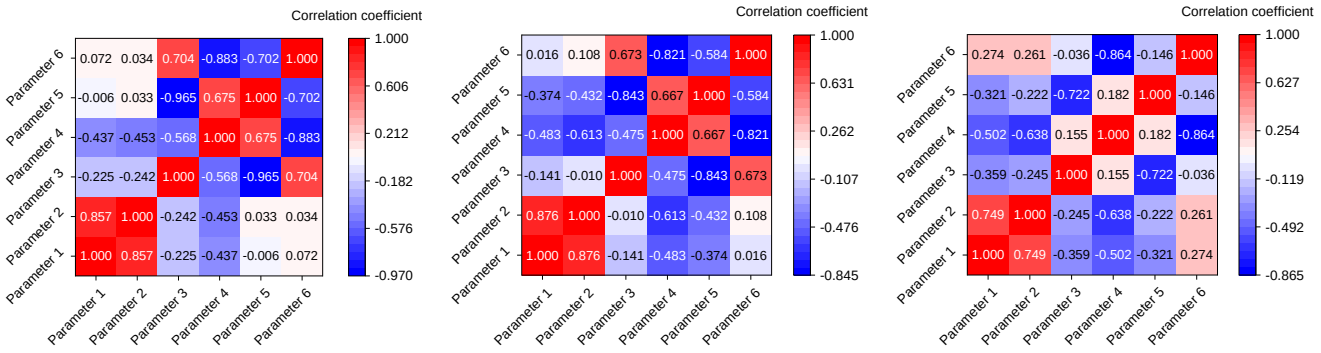

(a) End of Factorial DoE **(b)** End of MBDoE-MD **(c)** End of MBDoE-PP

Fig. 8 Correlation matrices of Model 3 at the end of Factorial DoE, MBDoE-MD and MBDoE-PP experimental campaigns.

for experiment 14. In experiment 14, the difference between the model predictions relative to the respective uncertainty limits is also significant for methane and carbon dioxide. This is shown in the joint prediction density plots in Figure 9. In the figure, the difference between the means of the prediction distributions of methane and carbon dioxide and also the difference between different observations of the two distributions (panels (a) and (c) of Figure 9) is greater than the standard deviation (half the error bound in the figure) of measurement error of methane and carbon dioxide. The result suggests that experiment 14 provided the only conditions where the models are significantly distinguishable. This aligns with the results suggested by the MBDoE-MD optimization, which also suggested experiment 14 provided the optimal conditions to discriminate between the two models. The prediction density plots also indicate that compared to Model 2, the observed values within their error bounds are less contradicted by Model 3. The residual plots of Model 2 and 3, showing the magnitude of prediction error (based on the final parameter estimates) at each experimental condition and for each of the output variables were also studied to compare with the results of prediction density plots. From the prediction density plots, prediction error or residuals can be computed as the difference between means of the distribution and the corresponding observed values. The residuals computed in this manner from the density plots are in alignment with the residuals shown in Figure 10, which are computed as the difference between model predictions and the observed values. The residual plots also suggested that both Model 2 and 3 had large residuals at experiments 5 and 12. A comparison of model predicted and experimental values for Model 3 at the end of the experimental campaign is provided in Figure 11 in the form of parity plots. As shown in the figure, Model 3 provides close predictions to the experimental data. Another interesting fact drawn from the figure is the narrow uncertainty intervals of predictions of the model evaluated from $\mathbf{V}_{\hat{\mathbf{y}}}(\cdot)$ computed using Equation 11. Compared to the uncertainty in measurements, the negligibly small uncertainty intervals of model predictions are reflected to the precise estimation of model parameters, which are the main source of uncertainty in model predictions. The details about computation of uncertainty intervals in panel (d) of Figure 11, which shows the parity plot of Model 3 in terms of methane conversion are provided in the SI.

4.4 Algorithm performance

The computational time for parameter estimation problems were close to 7 CPU seconds, whereas the solution of MBDoE problems took approximately 30 CPU seconds. Our implementation is available at `https://github.com/UCL/Methane_oxidation`.

5 Conclusions

An autonomous microreactor platform powered by optimal experimental design methods and data analysis was developed and successfully applied for kinetic model identification. The computational framework of the platform was developed in Python programming language and was integrated to a LabVIEW program controlling the microreactor system. A new Pyomo-based parameter estimation module was employed in the framework for the efficient solution of online parameter estimation problems. In addition, a probability criterion derived from the chi-square goodness of fit test was defined for online selection of appropriate models. The platform was successfully demonstrated on identifying an appropriate kinetic model along with precise estimation of its parameters for methane complete catalytic oxidation on Pd/Al_2O_3 catalyst. A total of 20 automated experiments were completed in two days for this purpose. Among the different kinetic models tested (Power law, Langmuir Hinshelwood and Mars van Krevelen), the Mars van Krevelen model was found to be the most appropriate, which agrees with similar studies reported in literature. The activation energies for the surface oxidation, surface reduction, and product formation steps of the Mars van Krevelen model were estimated to be 67.2, 95.1 and 79.8 kJ mol^{-1} respectively. Prediction density plots were employed as retrospective data analysis tools that are useful to review and reassess the decisions taken by the platform over time. In general, the prediction density plots together with experimental data provide insight about the uncertainty as well as adequacy of models in representing the data and their assumed distribution. The joint prediction density plots are also valuable tools to better understand the degree of discrimination between the competing models.

View Article Online
DOI: 10.1039/D3RE00156C

Table 8 The values of rate constant, pre-exponential factor and activation energies for different steps of Model 3

Reaction step	Rate constant at the reference temperature T_{ref}	Pre-exponential factor	Activation energy kJmol^{-1}
Surface oxidation	$k_1 = 3.12 \times 10^{-3}$ molbar^{-1} g^{-1} min^{-1}	2.58×10^{3} molbar^{-1} g^{-1} min^{-1}	$Ea_1 = 67.2$
Surface reduction	$k_2 = 2.82 \times 10^{-3}$ molbar^{-1} g^{-1} min^{-1}	6.69×10^{5} molbar^{-1} g^{-1} min^{-1}	$Ea_2 = 95.1$
Desorption of products	$k_3 = 3.83 \times 10^{-5}$ molg^{-1} min^{-1}	4.08×10^{2} molg^{-1} min^{-1}	$Ea_3 = 79.8$

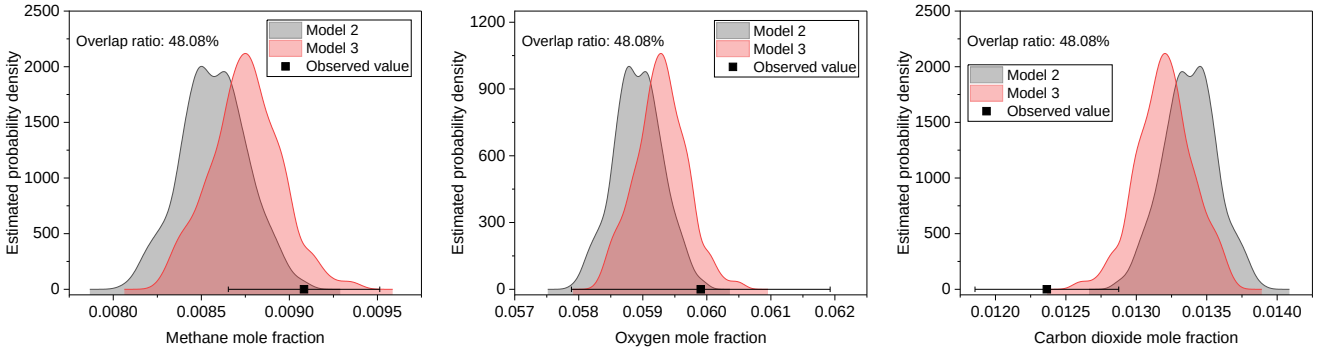

Fig. 9 Prediction density plots showing uncertainty in predictions of Model 2 and 3 at experiment 14 (reaction temperature = 325.9 ° C, mass flow rate = 27.7 Nml min^{-1}, oxygen/methane mole ratio = 3.9 mol mol^{-1}, inlet methane concentration = 0.022 mol mol^{-1}) for (a) Methane, (b) Oxygen and (c) Carbon dioxide. The observed value is shown as a point with the error bar (± standard deviation).

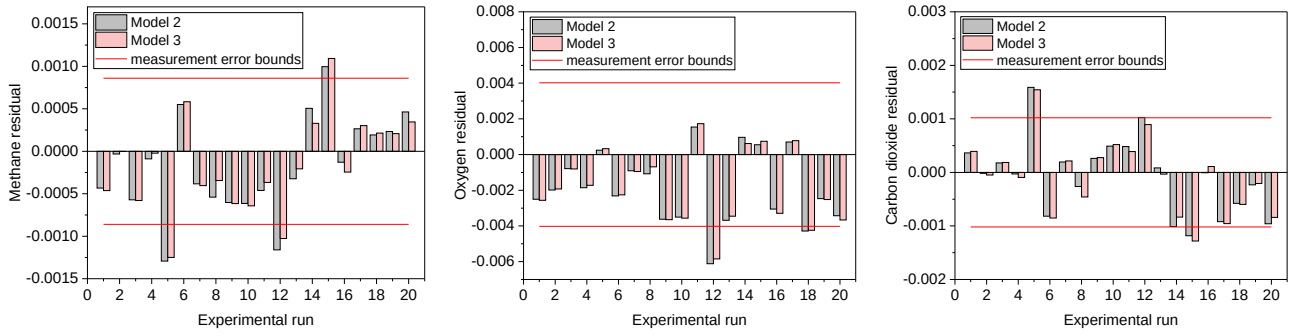

Fig. 10 Residual plots for Model 2 and 3 based on the final parameter estimates

.

View Article Online
DOI: 10.1039/D3RE00156C

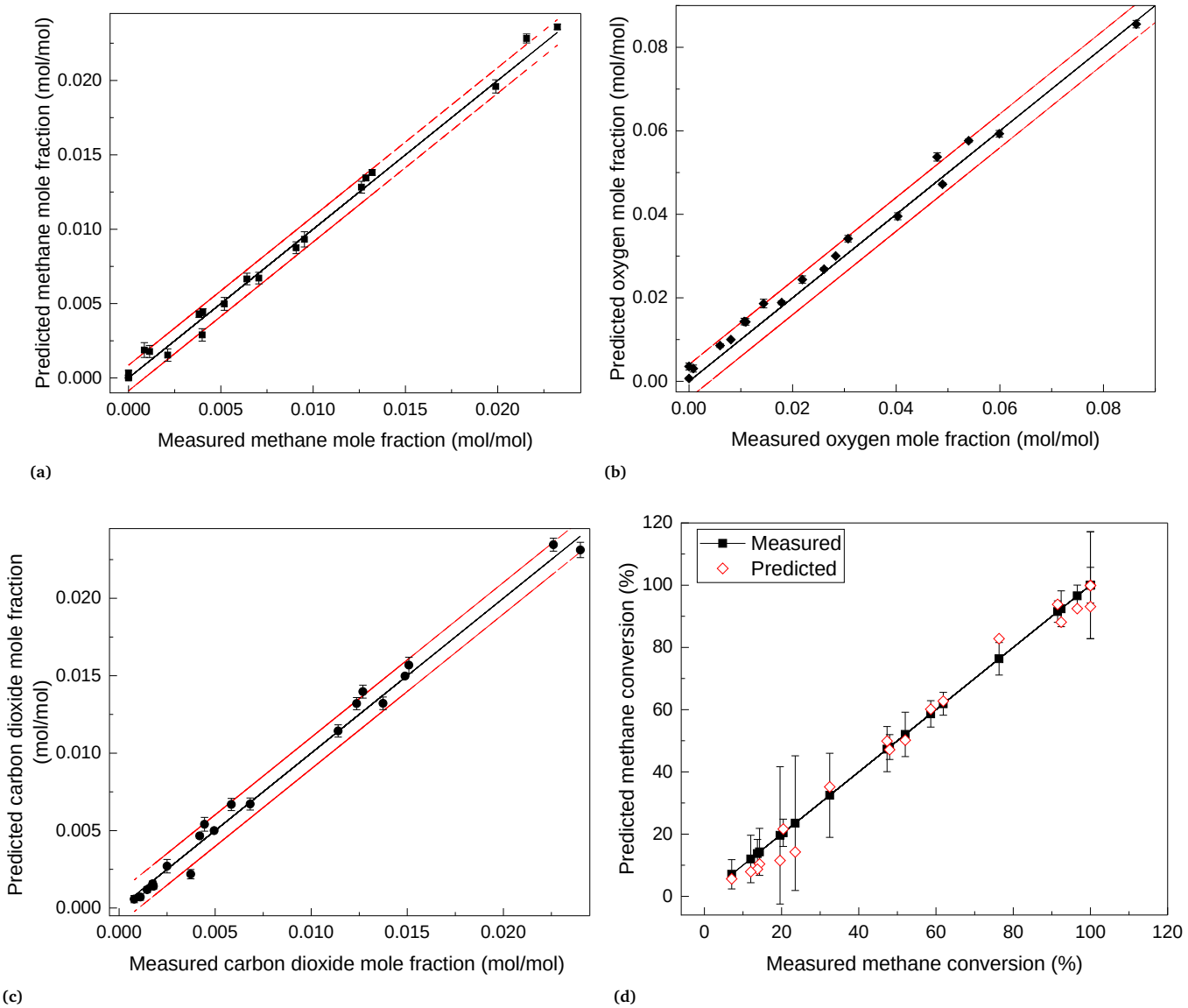

Fig. 11 Parity plots of Model 3 at the end of experimental campaign; i.e., at the end of experiment 20: (a) for methane, (b) for oxygen and (c) for carbon dioxide. In (a), (b) and (c), the black line represents the measured values, the two dotted red lines represent the measurement error ($\pm 2\times$ standard deviation). The model predictions are shown by the markers with the error bars, calculated as $\pm 2\times$ standard deviation of predictions. Panel (d) shows a comparison of experimental and predicted values of methane conversion. In (d), the line with squares represents the measured methane conversion with the corresponding error bars and the diamond markers represent the predicted values of methane conversion.

View Article Online
DOI: 10.1039/D3RE00156C

Conflicts of interest

There are no conflicts to declare.

Acknowledgements

A. Pankajakshan thanks the department of Chemical Engineering, University College London for his PhD studentship and S.G. Bawa thanks the Petroleum Technology Development Fund for his PhD studentship. We thank Johnson Matthey for providing the catalyst.

Glossary

Acronyms

CASP	Computer Aided Synthesis Planning
DAEs	Differential and Algebraic Equations
DoE	Design of Experiments
FIM	Fisher Information Matrix
GC	Gas Chromatography
GSD	Generalized Subset Design
GUI	Graphical User Interface
IPOPT	Interior Point OPTimizer
LH	Langmuir Hinshelwood
MBDoE	Model-based Design of Experiments
MBDoE-MD	MBDoE for model discrimination
MBDoE-PP	MBDoE for improving parameter precision
MVK	Mars van Krevelen
NLP	Nonlinear Programming
ODE	Ordinary Differential Equation
PFR	Plug Flow Reactor
Pyomo	Python Optimization Modeling Objects
RMG	Reaction Mechanism Generator
RMS	Reaction Modelling Suite
SLSQP	Sequential Least SQuares Programming

Latin Symbols

det	Determinant of a matrix
Ea	Activation energy
k	Reaction rate constant
n	Total number of samples
N	Total number of observations
$\mathcal{N}(\cdot,\cdot)$	Normal distribution with specified mean and variance
$N_{\mathbf{exp}}$	Number of performed experiments
N_θ	Number of model parameters
N_y	Number of response variables
$p(\cdot)$	Probability density function
$T_{ij}(\cdot)$	Objective function to discriminate between models i and j

Greek Symbols

α	Significance level
ε	Measurement error
θ_i	i-th model parameter
$\hat{\theta}_i$	Estimate of i-th model parameter
χ^2	Sum of squared residuals
$\psi(\cdot)$	Objective function of MBDoE-PP problem

Vectors and Matrices

$\mathbf{C_\theta}$	$[N_\theta \times N_\theta]$ parameter correlation matrix
$\mathbf{f}(\cdot)$	Vector of functions representing the state equation
$\mathbf{h}(\cdot)$	Vector of functions representing the output equation
$\mathbf{H_\theta}$	$[N_\theta \times N_\theta]$ Fisher information matrix
$\mathbf{T_{sp}}$	List of full set of sampling times (over all experiments)
$\mathbf{u}(\cdot)$	Vector $[N_u \times 1]$ of inputs or control variables
$\mathbf{U}$	List of full set of inputs (over all experiments)
$\mathbf{V}_{\hat{\mathbf{y}}}$	$[N_y \times N_y]$ covariance matrix of model predictions
$\mathbf{V_\theta}$	$[N_\theta \times N_\theta]$ parameter covariance matrix
$\mathbf{x}(\cdot)$	Vector of state variables
$\dot{\mathbf{x}}(\cdot)$	Vector of first derivatives of state variables
$\mathbf{y}(\cdot)$	Vector $[N_y \times 1]$ of outputs or response variables
$\hat{\mathbf{y}}(\cdot)$	Vector of model predictions of the output variables
$\mathbf{Y}$	List of full set of outputs (over all experiments)
$\Sigma_{\mathbf{Y}}$	Covariance matrix $[N_y \times N_y]$ of measurement error
$\boldsymbol{\theta}$	Vector $[N_\theta \times 1]$ of model parameters
$\boldsymbol{\varphi}$	Design vector

References

1 M. B. Plutschack, B. Pieber, K. Gilmore and P. H. Seeberger, *Chemical reviews*, 2017, **117**, 11796–11893.
2 A. Manz, N. Graber and H. á. Widmer, *Sensors and actuators B: Chemical*, 1990, **1**, 244–248.
3 K. F. Jensen, *Chemical Engineering Science*, 2001, **56**, 293–303.
4 S. Katare, *Comput. Aided Chem. Eng.*, 2003, **14**, 701–706.
5 C. W. Gao, J. W. Allen, W. H. Green and R. H. West, *Comput. Phys. Commun.*, 2016, **203**, 212–225.
6 M. Liu, A. Grinberg Dana, M. S. Johnson, M. J. Goldman, A. Jocher, A. M. Payne, C. A. Grambow, K. Han, N. W. Yee, E. J. Mazeau *et al.*, *J. Chem. Inf. Model.*, 2021, **61**, 2686–2696.
7 N. M. Vandewiele, K. M. Van Geem, M.-F. Reyniers and G. B. Marin, *Chem. Eng. J.*, 2012, **207**, 526–538.
8 P. S. Mendes, S. Siradze, L. Pirro and J. W. Thybaut, *React. Chem. Eng.*, 2022, **7**, 142–155.
9 C. W. Coley, N. S. Eyke and K. F. Jensen, *Angew. Chemie-Int. Ed.*, 2020, **59**, 22858–22893.
10 C. W. Coley, N. S. Eyke and K. F. Jensen, *Angew. Chemie-Int. Ed.*, 2020, **59**, 23414–23436.
11 C. W. Coley, D. A. Thomas III, J. A. Lummiss, J. N. Jaworski, C. P. Breen, V. Schultz, T. Hart, J. S. Fishman, L. Rogers, H. Gao *et al.*, *Science*, 2019, **365**, eaax1566.
12 A. Echtermeyer, Y. Amar, J. Zakrzewski and A. Lapkin, *Beilstein J. Org. Chem.*, 2017, **13**, 150–163.
13 A. M. Schweidtmann, A. D. Clayton, N. Holmes, E. Bradford, R. A. Bourne and A. A. Lapkin, *Chem Eng. J.*, 2018, **352**, 277–282.

View Article Online
DOI: 10.1039/D3RE00156C

14 C. A. Hone, N. Holmes, G. R. Akien, R. A. Bourne and F. L. Muller, *React. Chem. Eng.*, 2017, **2**, 103–108.

15 J. S. Moore and K. F. Jensen, *Org. Process Res. Dev.*, 2012, **16**, 1409–1415.

16 B. J. Reizman, Y.-M. Wang, S. L. Buchwald and K. F. Jensen, *React. Chem. Eng.*, 2016, **1**, 658–666.

17 R. A. Fisher, *The design of experiments*, Oliver & Boyd, Edinburgh, 1935.

18 G. E. Box and H. Lucas, *Biometrika*, 1959, **46**, 77–90.

19 G. E. Box and N. R. Draper, *Empirical model-building and response surfaces.*, John Wiley & Sons, Blackwell, 1987.

20 S. Asprey and S. Macchietto, *Comput. Chem. Eng.*, 2000, **24**, 1261–1267.

21 G. Franceschini and S. Macchietto, *Chem. Eng. Sci.*, 2008, **63**, 4846–4872.

22 J. P. McMullen and K. F. Jensen, *Org. Process Res. Dev.*, 2011, **15**, 398–407.

23 B. J. Reizman and K. F. Jensen, *Org. Process Res. Dev.*, 2012, **16**, 1770–1782.

24 S. D. Schaber, S. C. Born, K. F. Jensen and P. I. Barton, *Org. Process Res. Dev.*, 2014, **18**, 1461–1467.

25 C. Waldron, A. Pankajakshan, M. Quaglio, E. Cao, F. Galvanin and A. Gavriilidis, *React. Chem. Eng.*, 2019, **4**, 1623–1636.

26 C. Waldron, A. Pankajakshan, M. Quaglio, E. Cao, F. Galvanin and A. Gavriilidis, *React. Chem. Eng.*, 2020, **5**, 112–123.

27 M. Quaglio, C. Waldron, A. Pankajakshan, E. Cao, A. Gavriilidis, E. S. Fraga and F. Galvanin, *Comput. Chem. Eng.*, 2019, **124**, 270–284.

28 C. Waldron, A. Pankajakshan, M. Quaglio, E. Cao, F. Galvanin and A. Gavriilidis, *Ind. Chem. Eng. Res.*, 2019, **58**, 22165–22177.

29 C. J. Taylor, H. Seki, F. M. Dannheim, M. J. Willis, G. Clemens, B. A. Taylor, T. W. Chamberlain and R. A. Bourne, *React. Chem. Eng.*, 2021, **6**, 1404–1411.

30 M. N. Cruz Bournazou, T. Barz, D. Nickel, D. C. Lopez Cárdenas, F. Glauche, A. Knepper and P. Neubauer, *Biotechnol. Bioeng.*, 2017, **114**, 610–619.

31 W. E. Hart, J.-P. Watson and D. L. Woodruff, *Math. Program. Comput.*, 2011, **3**, 219–260.

32 M. L. Bynum, G. A. Hackebeil, W. E. Hart, C. D. Laird, B. L. Nicholson, J. D. Siirola, J.-P. Watson, D. L. Woodruff *et al.*, *Pyomo-optimization modeling in Python*, Springer, Cham, Switzerland, 2021.

33 B. Nicholson, J. D. Siirola, J.-P. Watson, V. M. Zavala and L. T. Biegler, *Math. Program. Comput.*, 2018, **10**, 187–223.

34 I. Surowiec, L. Vikstrom, G. Hector, E. Johansson, C. Vikstrom and J. Trygg, *Analytical chemistry*, 2017, **89**, 6491–6497.

35 S. G. Bawa, A. Pankajakshan, C. Waldron, E. Cao, F. Galvanin and A. Gavriilidis, *Chemistry-Methods*, 2023, **3**, e202200049.

36 R. A. Fisher, *Philosophical Transactions of the Royal Society of London. Series A, Containing Papers of a Mathematical or Physical Character*, 1922, **222**, 309–368.

37 Y. Bard, *Nonlinear parameter estimation*, Academic Press, New York, 1974.

38 A. B. Singer, J. W. Taylor, P. I. Barton and W. H. Green, *J. Phys. Chem. A*, 2006, **110**, 971–976.

39 R. Ramachandran and P. I. Barton, *Chem. Eng. Sci.*, 2010, **65**, 4884–4893.

40 H. G. Bock, S. Körkel and J. P. Schlöder, in *Model Based Parameter Estimation: Theory and Applications*, ed. H. G. Bock, T. Carraro, W. Jäger, S. Körkel, R. Rannacher and J. P. Schlöder, Springer, Berlin, Heidelberg, 2013, ch. Parameter Estimation and Optimum Experimental Design for Differential Equation Models, pp. 1–30.

41 L. T. Biegler, *Nonlinear programming: concepts, algorithms, and applications to chemical processes*, SIAM, 2010.

42 R. A. Fisher, *Statistical methods for research workers*, Oliver & Boyd, Edinburgh, 11th edn, 1950.

43 J. Neyman and E. S. Pearson, *Philosophical Transactions of the Royal Society of London. Series A, Containing Papers of a Mathematical or Physical Character*, 1933, **231**, 289–337.

44 K. Pearson, *The London, Edinburgh, and Dublin Philosophical Magazine and Journal of Science*, 1900, **50**, 157–175.

45 Student, *Biometrika*, 1908, **6**, 1–25.

46 A. Saltelli, S. Tarantola, F. Campolongo and M. Ratto, *Sensitivity analysis in practice: a guide to assessing scientific models*, Wiley, New York, 2004.

47 A. Saltelli, M. Ratto, T. Andres, F. Campolongo, J. Cariboni, D. Gatelli, M. Saisana and S. Tarantola, *Global sensitivity analysis: the primer*, John Wiley & Sons, Chichester, West Sussex, 2008.

48 I. Sokolović, M. Reticcioli, M. Čalkovskỳ, M. Wagner, M. Schmid, C. Franchini, U. Diebold and M. Setvín, *Proc. Natl. Acad. Sci.*, 2020, **117**, 14827–14837.

49 M. Schwaab, F. M. Silva, C. A. Queipo, A. G. Barreto Jr, M. Nele and J. C. Pinto, *Chem. Eng. Sci.*, 2006, **61**, 5791–5806.

50 G. B. Ferraris, P. Forzatti, G. Emig and H. Hofmann, *Chem. Eng. Sci.*, 1984, **39**, 81–85.

51 E. Walter and L. Pronzato, *Identification of parametric models from experimental data*, Springer Verlag, New York, 1997.

52 C. J. Kalkman, *J. Clin. Monit.*, 1995, **11**, 51–58.

53 R. Bitter, T. Mohiuddin and M. Nawrocki, *LabVIEW: Advanced programming techniques*, CRC Press, Boca Raton, 2017.

54 C. Elliott, V. Vijayakumar, W. Zink and R. Hansen, *J. Lab. Autom.*, 2007, **12**, 17–24.

55 G. Ertl, H. Knözinger, J. Weitkamp *et al.*, *Handbook of heterogeneous catalysis*, VCH, Weinheim, 1997.

56 S. Specchia, F. Conti and V. Specchia, *Ind. Eng. Chem. Res.*, 2010, **49**, 11101–11111.

57 P. Hurtado, S. Ordóñez, H. Sastre and F. V. Dıez, *Appl. Catal. B Environ.*, 2004, **51**, 229–238.

58 S. P. Asprey and Y. Naka, *J. Chem. Eng. Japan*, 1999, **32**, 328–337.

59 G. Buzzi-Ferraris and F. Manenti, *Chem. Eng. Sci.*, 2009, **64**, 1061–1074.

60 R. Sjoegren, *Design of experiments for Python*, https://pypi.org/project/pyDOE2/, accessed May 2023.

View Article Online
DOI: 10.1039/D3RE00156C

61 P. Virtanen, R. Gommers, T. E. Oliphant, M. Haberland, T. Reddy, D. Cournapeau, E. Burovski, P. Peterson, W. Weckesser, J. Bright *et al.*, *Nat. Methods*, 2020, **17**, 261–272.
62 A. C. Hindmarsh, *Sci. Comput.*, 1983, 55–64.
63 A. Wächter and L. T. Biegler, *Math. Program.*, 2006, **106**, 25–57.
64 D. Kraft, *Technical Report DFVLR-FB*, 1988.